Int. J. Heat Mass Transfer. Vol. 16, pp. 1785–1795. Pergamon Press 1973. Printed in Great Britain

NATURAL CONVECTION FLOW PATTERNS IN SPHERICAL ANNULI

S. H. YIN
Chung Yuan Christian College of Science and Engineering, Chung Li, Taiwan
R. E. POWE, J. A. SCANLAN and E. H. BISHOP
Montana State University, Bozeman, Montana, U.S.A.

(*Received* 27 *December* 1972 *and in revised form* 8 *March* 1973)

Abstract—An experimental investigation is described concerning the natural convection flow patterns which occur in the annular space between two concentric isothermal spheres, the inner one being hotter. The diameter ratios ranged from 1·09 to 2·17. The convecting fluids were air and water, yielding Grashof numbers in the range of $1{\cdot}7 \times 10^3$ to $1{\cdot}5 \times 10^7$. The several types of flow patterns observed are correlated with previously published temperature profiles and are categorized in terms of steady and unsteady regimes.

NOMENCLATURE

- D, diameter;
- g, local gravitational acceleration;
- Gr, Grashof number defined by equation (1);
- L, gap width, $r_0 - r_i$;
- r, radius;
- r_{av}, average radius, $(r_i + r_0)/2$;
- T, temperature;
- T_m, volume-weighted mean temperature defined by equation (2);
- β, thermal expansion coefficient;
- ΔT, temperature difference, $T_i - T_0$;
- ν, kinematic viscosity.

Subscripts

- i, outer surface of inner sphere;
- 0, inner surface of outer sphere.

1. INTRODUCTION

In 1964, the first paper dealing with natural convection flow between isothermal concentric spheres appeared in the literature [1]. In this paper, Bishop *et al.* reported on the flow patterns observed for air as the working fluid. Photographs and qualitative descriptions of two steady patterns, the crescent eddy and the kidney-shaped eddy, and one unsteady pattern, falling vortices, were presented. While additional papers [2, 4, 6] concerning natural convection between isothermal spheres have recently been published, the results presented in these papers dealt with overall heat transfer rates and thermal field data with no additional information on the flow phenomena *per se*.

The purpose of the present paper is to present additional results on the flow between isothermal concentric spheres. These results are for air as the working fluid for diameter ratios intermediate to those reported in [1] and for water as the working fluid. Photographs and detailed qualitative descriptions of the flow observed are presented for diameter ratios of 1·09, 1·40, 1·78 and 2·17 and for Grashof numbers between $1{\cdot}7 \times 10^3$ and $1{\cdot}5 \times 10^7$. The photographs of the patterns observed for water are to the authors' knowledge the first reported in the literature for natural convection of water in confined spaces. The technique for making the patterns photographable is described.

2. APPARATUS AND PROCEDURE

The flow visualization apparatus, Figs. 1 and 2,

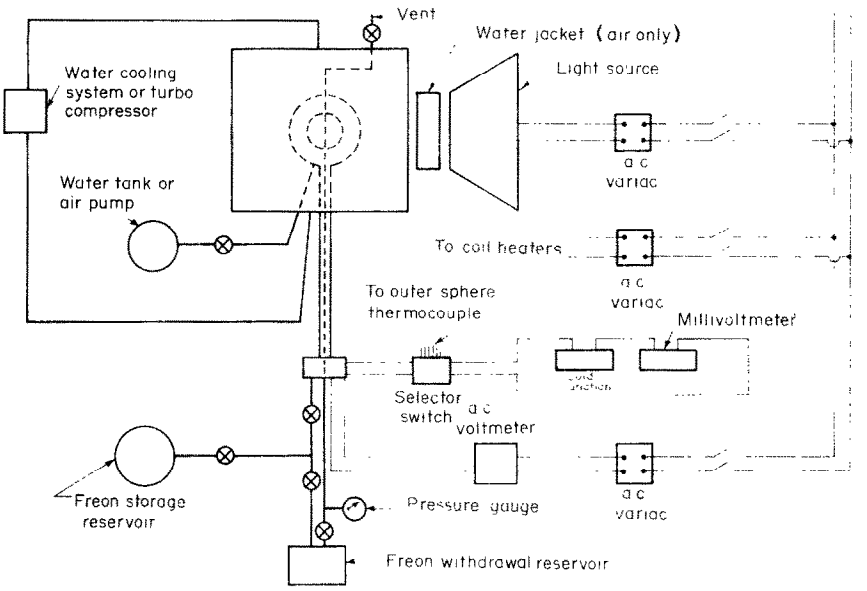

FIG. 2. Flow visualization apparatus.

consisted of two concentric spheres enclosed in a cubical enclosure [8]. Values of diameter ratio of 1·09, 1·40, 1·78 and 2·17 were obtained by utilizing inner spheres of 11·43, 13·97, 17·78 and 22·86 cm o.d. in conjunction with a single outer sphere of 24·82 cm i.d. The inner spheres were 0·064 cm thick copper and the outer sphere was 0·53 cm thick glass.

The inner spheres, which were painted flat black to minimize reflections, were supported in the outer sphere by a 1·27 cm dia stainless steel stem which was insulated on its lateral surface. The inner sphere surface temperature was kept uniform by condensing Freon-11 vapor on the inner surface on the sphere. The saturation conditions of the Freon were varied by changing the power input to electrical disk heaters located within the inner sphere below the liquid level. Thermocouples placed at 90° intervals around the horizontal equator of the sphere were used to measure the temperature of the inner sphere. A small stainless steel tube extended through the support stem for pressure measurements within the inner sphere and for venting during Freon charging.

The outer sphere consisted of two glass hemispheres joined together using a silicone sealant which yielded leak-proof sealing and ease of disassembly for changing the inner sphere. The joint of the two hemispheres was located at an angle of 30° with respect to the vertical axis. Proper positioning of the sphere in the cubical enclosure then permitted unobstructed viewing of the entire right half of the gap between the two spheres. Approximately three-fourths of the surface of the glass sphere was painted flat black to reduce light reflections. A small hole at the top of the outer sphere served as an air vent while the gap was being filled with water and as a vent to the atmosphere when air was used as the test fluid. Six thermocouples, embedded the depth of the wall thickness, were attached to the glass sphere with epoxy cement, and the surface temperature was taken to be the average of these six thermocouple readings. A cylindrical plexiglass spacer, through which passed the inner sphere support stem and tubes for charging the gap with water and tracer particles, was attached to the bottom of the outer sphere by epoxy cement. The spacer

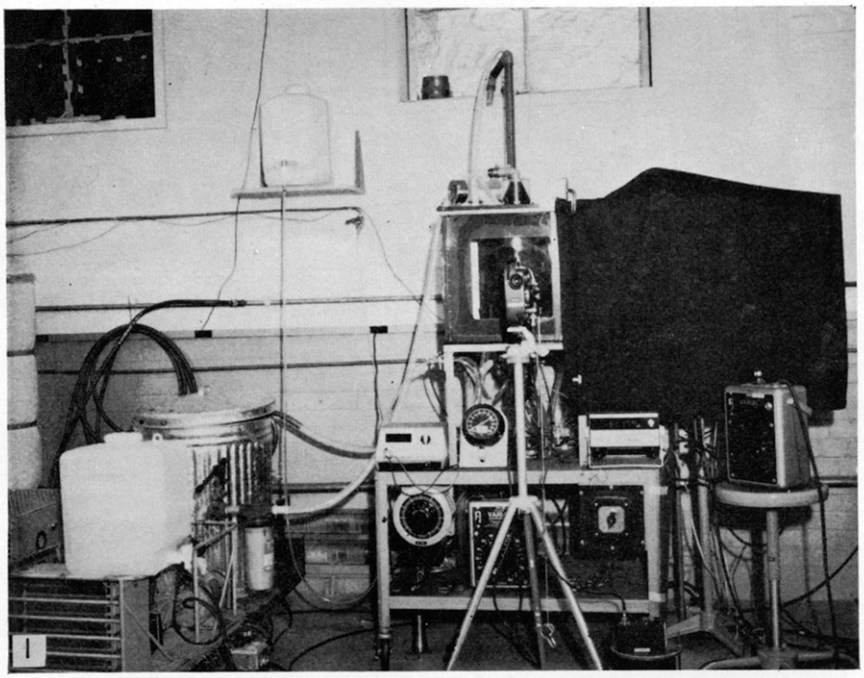

FIG. 1. Flow visualization apparatus.

[*facing page* 1786]

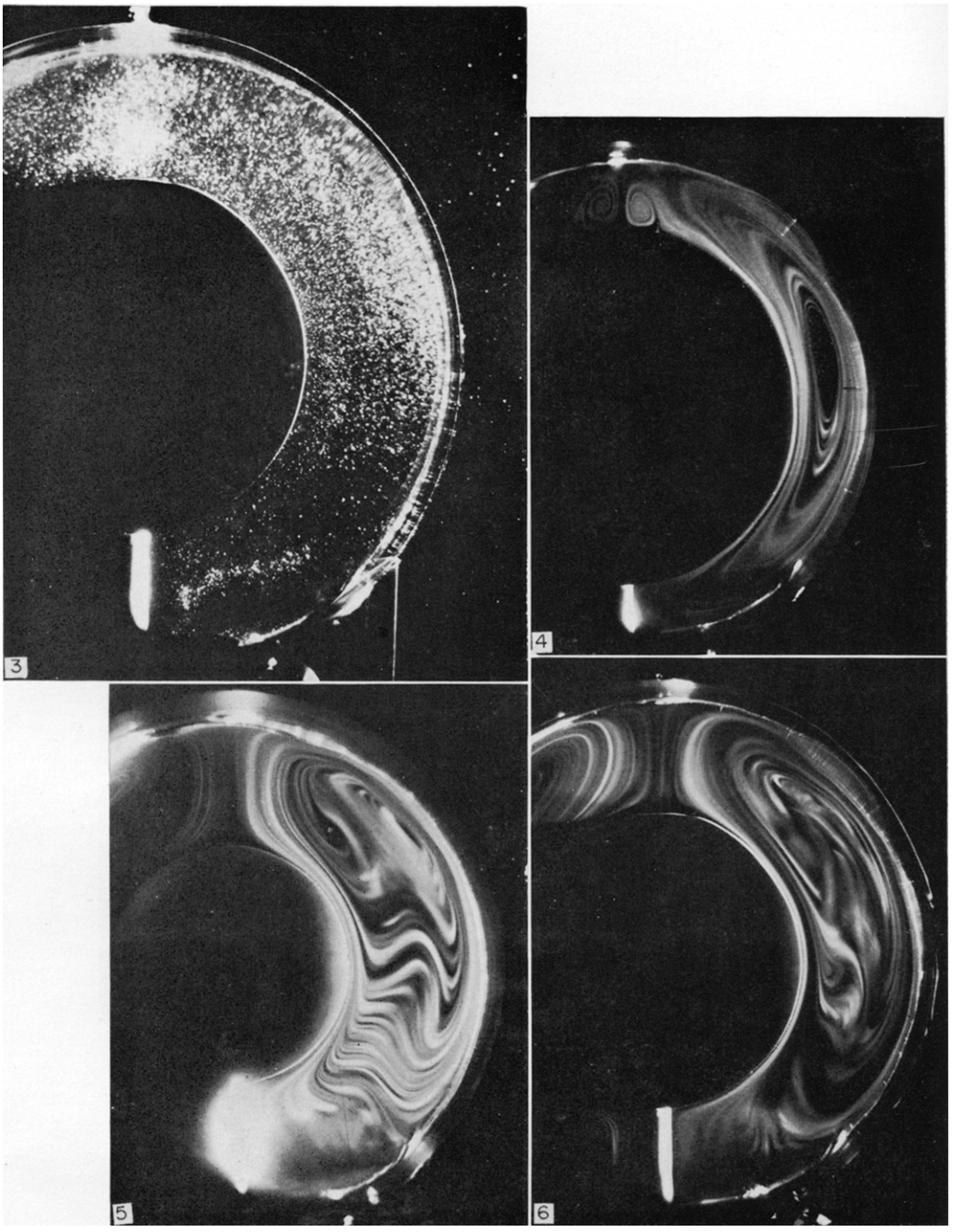

FIG. 3. Particles suspended in water with no impressed temperature difference.
FIG. 4. Steady flow pattern in air for $D_o\ D_i = 1{\cdot}40$ and $Gr = 8\,400$.
FIG. 5. Unsteady flow pattern in air for $D_o\ D_i = 2{\cdot}17$ and $Gr = 1\,056\,000$.
FIG. 6. Unsteady flow pattern in air for $D_o\ D_i = 1{\cdot}78$ and $Gr = 323\,000$.

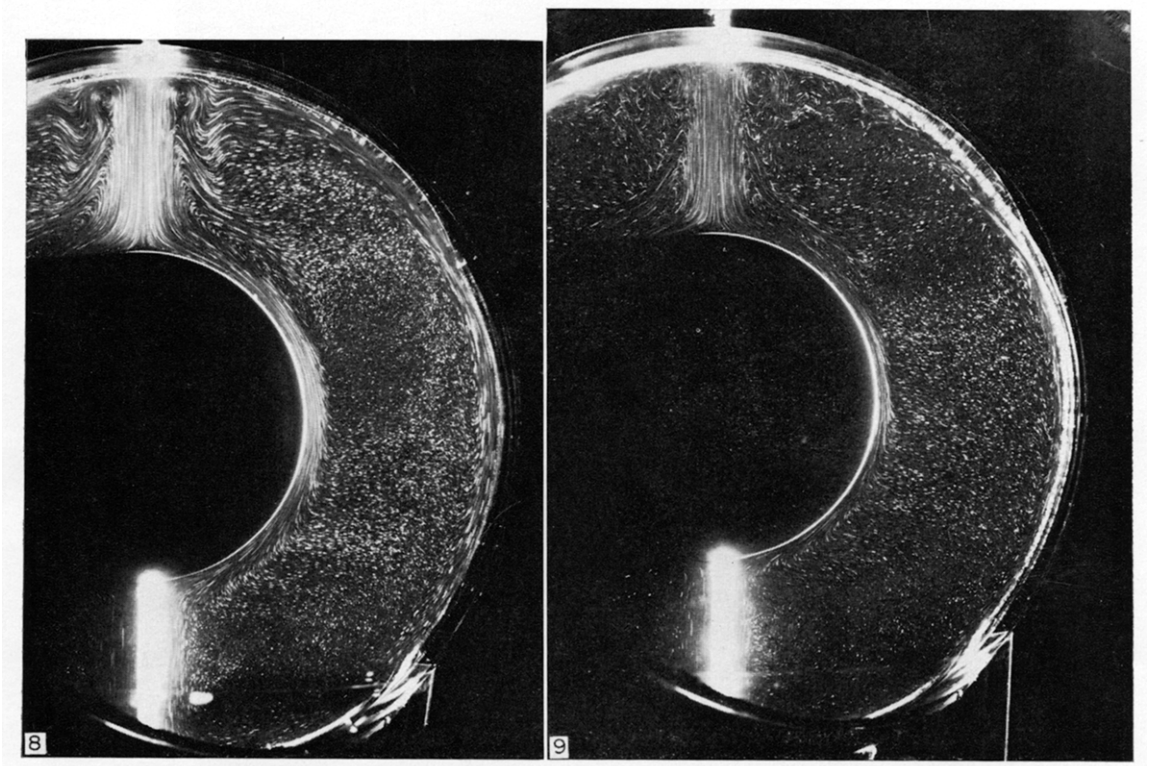

FIG. 8. Basic steady flow pattern in water for $D_o/D_i = 2{\cdot}17$ and $Gr = 248\,800$.

FIG. 9. Unsteady flow pattern in water for $D_o/D_i = 2{\cdot}17$ and $Gr = 3\,600\,000$.

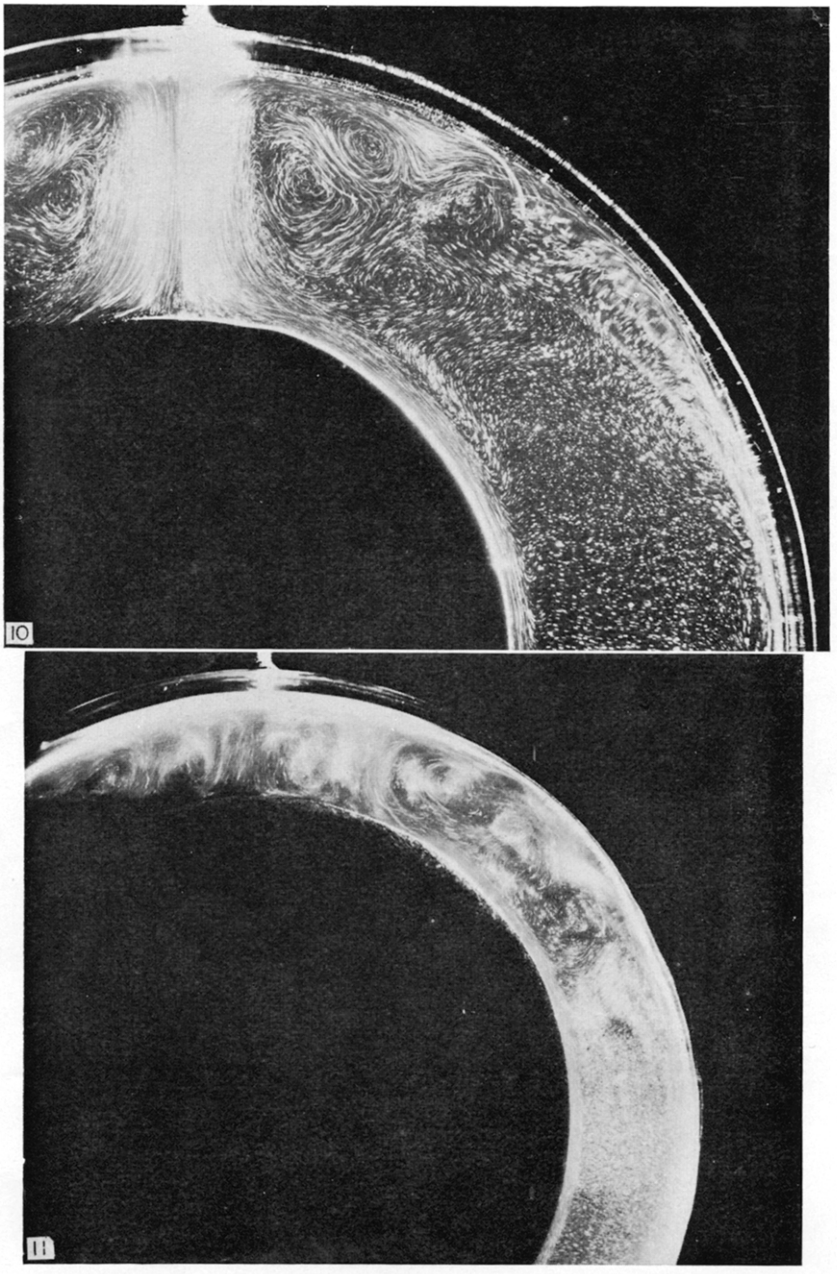

FIG. 10. Unsteady flow pattern in water for $D_o/D_i = 1{\cdot}78$ and $Gr = 1\,688\,000$.

FIG. 11. Unsteady flow pattern in water for $D_o/D_i = 1{\cdot}40$ and $Gr = 2\,497\,000$.

was attached to the bottom of the cubical enclosure by screws.

The cubical enclosure was made of 1·27 cm thick plexiglass and had a characteristic length of 45·7 cm. To permit changing of the spheres, the enclosure was designed so that the top cover could be easily removed. In order to minimize optical reflections, the inner surfaces of the cubical enclosure were lined with thin phenolic sheets painted flat black with the exception of a viewing port and a 0·5 cm vertical lighting slit.

The outer sphere was maintained in an isothermal condition by a forced air draft or circulating water depending upon which was being used as the gap test fluid. The forced air draft, produced by a turbo-compressor, was introduced into the cubical enclosure by a manifold arrangement from both the top and bottom of the enclosure and was withdrawn through a narrow gap underneath the edges of the top cover. This arrangement tended to eliminate flow separation of the cooling air while passing over the glass sphere, and thus permit better control of the isothermality of the glass sphere. The water circulation system was composed of a reservoir, pump, filter, and chiller and was operated at a flow rate of approximately 0·32 l/s (5 gal/min). The cooling water was introduced into the cubical enclosure at the top and withdrawn at the bottom through a manifold system. A thin plastic cylinder 30·5 cm dia was attached to the bottom of the enclosure with its axis coincident with the vertical axis of the supporting stem and extended up almost to the horizontal diameter of the glass sphere. At this location, a narrow gap existed between the sphere and the cylinder. Two coil heaters connected to an a.c. Variac were placed within the cylinder surrounding the plexiglas spacer which held the glass sphere to the cubical enclosure. The outlet mainfold openings in the bottom of the enclosure were located outside of this cylinder so that the cooling water in the region directly beneath the sphere would remain stagnant until energy was supplied to the coil heaters. This arrangement was necessary since the temperature of the inner surface of the glass sphere in the lower region would tend to be several degrees cooler than in the upper region. Isothermality was achieved by varying the power input to the coil heaters until satisfactory thermal conditions were achieved on the inner surface of the sphere. The use of water as the cooling fluid when water was used as the gap test fluid eliminated distortions which would be caused by refraction at the curved water–glass–cooling fluid interfaces if air had been used instead.

The inner-sphere support-stem passed through the outer glass sphere and the cubical enclosure through O-ring seals and was connected to a small cylindrical, stainless steel reservoir. The reservoir provided means of connecting electrical leads to the disk heaters, leads to the inner-sphere surface thermocouples, and the pressure probe to instrumentation; it also provided means for charging the inner sphere with Freon-11. The reservoir rested on a threaded rod which was used to position the inner sphere along the vertical diameter within the outer sphere.

A thin vertical collimated plane of light from two 650 W, air cooled, high intensity, quartz–iodine lamps passed through the center of the concentric spheres. After the injection of tracer particles into the gap, this permitted visual and photographic observation of the flow in a plane by viewing at right angles to the collimated light beam. When air was used as the gap test fluid, the light beam was passed through a 1·9 cm thick plane of water to reduce the radiant heating of the air by the high intensity light; when water was used as the test fluid, the circulating cooling water in the cubical enclosure served the same purpose.

Tobacco (cigar) smoke was used to make the flow visible when air was the test fluid. The smoke was introduced into the gap through small tubes positioned beside the inner-sphere support stem.

Visualizing the natural convective flow of water in a confined space presents a unique and

very difficult experimental problem. Several different kinds of solid particles used by previous investigators were evaluated. Some of these were aluminum powders, polyethylene, polystyrene, and small hollow glass spheres. These particles revealed some or all of the following disadvantages:

(1) They did not remain neutrally buoyant for an extended period of time under the necessary variation of water temperature.

(2) They adhered to the inner surface of the glass sphere which reduced the optical quality significantly.

(3) They were poor reflectors of light.

A flow visualization technique described by Baker [7] was also tried but proved to be ineffective. In this technique a small amount of thymol blue pH indicator is added to the water, and a small d.c. voltage is impressed between two electrodes within the solution. This creates a blue dye in the gap, which follows the convective currents; however, the contrast between the blue dye and the red tint of the water and the thymol solution is poor.

It was found that by adding several drops of a particular liquid detergent to deaerated distilled water and gently vibrating the mixture to form a homogeneous solution, numerous very small neutrally buoyant particles appeared after the solution remained motionless for several hours. Figure 3 shows these particles in the gap with no temperature difference impressed between the spheres. The time exposure for this photograph was 8 s. The particle concentration could be changed by simply increasing or reducing the amount of detergent added to the water; however, too much detergent caused the water to become milky gray. The number of particles obtained is also a function of the average temperature of the water with a temperature of 120°F apparently the maximum which will yield satisfactory results. Additional work needs to be done to determine the relationship between detergent amounts and temperature. After filtration of the detergent–water solution, it was found that the particles were approximately 5–15 μ in size, and microscopic study showed that they were very irregular in shape. Apparently this accounts for their excellent optical reflectivity. To the authors' knowledge, this particular flow visualization technique has not been reported in the literature, and the photographs of natural convective flow of water in a confined space contained in this paper are the first to be published.

Still photographs of the flow patterns were obtained using a tripod-mounted 4 in. × 5 in. Calumet Camera, and motion pictures were taken by use of a Beaulieu R 16 mm "Automatic" photographic recorder. Kodak 4-X Reversal, 7277 16 mm movie film was used for the motion pictures. All of the still photographs were taken with either Kodak Tri-X Pan Professional Film or Polaroid Black and White 3000 speed Land film. In order to achieve good contrast, kodabromide F.4 print paper was used for enlargement and printing.

The procedure used in visualizing the flow patterns was as follows. First, the temperature difference between the spheres was adjusted by varying the power input to the disk heaters, the cooling fluid temperature and flow rate, and the power input to the coil heaters when water was used as the cooling fluid. For air as the gap test-fluid, tobacco smoke was then gently introduced into the gap and sufficient time was allowed to insure stability and equilibrium of the flow pattern. For water as the gap test-fluid, tracer particles were already contained in the water since the detergent was added to the water prior to placement into the spherical annulus. After the flow pattern had stabilized, both still and motion pictures were taken.

Table 1 gives the range of Grashof numbers achieved for each of the diameter ratios studied.

For the purpose of correlating with previous heat transfer work [4], the Grashof numbers in Table 1 were calculated as

$$Gr = g\beta L^3(\Delta T)/\nu^2 \qquad (1)$$

wherein the fluid properties were evaluated at a volume-weighted mean temperature defined by

$$T_m = [(r_{av}^3 - r_i^3)T_i + (r_0^3 - r_{av}^3)T_0]/(r_0^3 - r_i^3). \quad (2)$$

Table 1. Range of Grashof numbers obtained for each diameter ratio and test fluid

Diameter ratio	Gap fluid	Gr_{min}	Gr_{max}
1·09	water	$1·7 \times 10^3$	$7·7 \times 10^4$
1·40	air	$7·0 \times 10^3$	$1·2 \times 10^5$
1·40	water	$5·8 \times 10^4$	$5·5 \times 10^6$
1·78	air	$4·2 \times 10^4$	$6·2 \times 10^5$
1·78	water	$1·5 \times 10^5$	$5·6 \times 10^6$
2·17	air	$7·2 \times 10^4$	$1·2 \times 10^6$
2·17	water	$1·5 \times 10^5$	$1·5 \times 10^7$

3. DISCUSSION OF RESULTS

For air as the gap working fluid, the basic flow pattern obtained for all sphere combinations at low Grashof numbers is a steady crescent eddy flow pattern as previously observed for both concentric spheres [1] and for concentric cylinders [3]. In this pattern, the fluid immediately adjacent to the spheres flows with a relatively high speed compared to that in the central and major portion of the gap. Flow is upward along the inner sphere and downward along the outer sphere. A distinct center of the crescent eddy is observed, and, in the upper region of the gap, there exists a distinct vertical dividing line, or chimney, between the two symmetrical halves of the pattern. It was observed that the location of the eddy center moved radially outward and upward in angular position for an increase in Grashof number with a given sphere combination.

The only exception to the occurrence of the simple crescent eddy pattern at low Grashof numbers is for the smallest diameter ratio utilized with air, 1·40. Although the simple crescent eddy pattern occurs for Grashof numbers above 12000, the main flow does not extend completely into the upper portion of the annulus for Grashof numbers between 7000 and 12000, as shown in Fig. 4. This results in two small secondary cells forming in the extreme upper portion of the annulus—one to either side of the sphere's vertical axis. It should be noted that, for a steady, two-dimensional flow pattern, fluid cannot be continually fed into the two small cells, as appears to be the case in Fig. 4. This appearance results from the fact that the photograph was taken before the flow had become fully developed. However, if enough time were allowed for the fully developed condition to be attained, the smoke had diffused to such an extent that high quality photographs were not obtainable, although the two secondary cells were still observable. These cells are completely stationary in size and location, and each of them rotates counter to both the large adjacent eddy and the adjacent secondary cell. It should be kept in mind that photographs, such as that shown in Fig. 4, are thin plane sections through flow patterns in circular, three-dimensional, annular space.

For the two larger diameter ratios studied using air as the test fluid, 2·17 and 1·78, a second steady flow pattern, the kidney-shaped eddy pattern, occurs for moderate Grashof numbers. As had been previously observed for both concentric spheres [1] and concentric cylinders [3], this pattern is characterized by a distortion of the central flow region into a distinct kidney shape, while the thin, high-speed layers near the sphere surfaces remain relatively unchanged. The distortion of the central low-speed region becomes more pronounced as the Grashof number is increased.

For all sphere combinations utilized in the current investigation, an unsteady flow pattern occurs when the Grashof number exceeds a transition value, and the exact nature of the unsteady flow was found to be dependent on the diameter ratio. It should be noted that, for Grashof numbers only slightly above the transition value, very small deviations from steady flow were observed. In fact, the transition Grashof number is defined as the smallest value of the Grashof number for which any unsteadiness can be observed in the flow field. As the

Grashof number is increased above the transition value, however, the unsteadiness becomes increasingly more pronounced.

For the largest diameter ratio utilized in the current study with air as the test fluid, 2·17, the unsteadiness above the transition Grashof number consists of a continuous radial wave motion observed in the central low-speed flow region as shown in Fig. 5. This wave motion is characterized by a continuous shifting of the flow lines in the radial direction from the vicinity of the eddy center toward the inner sphere. This radially inward-shifting flow combines with part of the upward flow and then returns to the lower portion of the low-speed central region through the area immediately adjacent to the outer sphere high-speed layer. During these occurrences, both the eddy center and the vertical chimney remain distinct and stationary in the flow field, and neither the inner nor the outer sphere high speed layer is disrupted to any observable degree by the unsteadiness in the central portion of the gap.

For the intermediate diameter ratio utilized with air as the test fluid, 1·78, the steady flow pattern exists undisturbed until a Grashof number of about 246000 is reached. At this point, a periodic contraction, with an irregular period of occurrence, is found in the lower portion of the central flow region. For a value of the Grashof number of about 275 000, this interior contraction motion becomes more violent, and a radial shifting of the flow lines begins to occur in the central portion of the gap. At this point, the center of the eddy still remains visible, but when the Grashof number is increased above approximately 317 000, the center of the eddy is no longer distinct, and a very slight tangential oscillation of the chimney is produced by the violent motion in the central portion of the gap. As in the previous case, however, the thin high-speed layers near the inner and outer spheres are relatively undisturbed by the unsteadiness in the central gap region. Throughout this range of Grashof numbers, the rate of occurrence of the interior contraction increases as the Grashof number is increased. This type of flow pattern is illustrated in Fig. 6.

The final unsteady flow pattern, which was observed for the smallest diameter ratio used with air as the test fluid, is characterized by the following motions. The high-speed flow along the surface of the inner sphere breaks away from the surface and shoots into the upper portion of the annulus resulting in rolling vortices in counter-rotation with each other. These cells are associated with sideways oscillations about the vertical, and occasionally the cells are disrupted but are immediately reformed. Due to this sideways oscillation in the upper portion of the gap, a slight tangential motion is impressed on the large primary cell. It should be noted that for this unsteady flow pattern, the chimney along the upward vertical axis no longer exists.

Following disruption of the rolling vortices, the fluid in the upper region of the gap flows downward via the inner surface of the outer sphere, returning to the lower portion of the annulus with a three-dimensional spiral motion. There is no distinct center of the primary eddy in the lower portion of the gap, and flow lines do not maintain a constant position but are shifted in the radial direction. This appears to be caused by large slugs of fluid flowing from the upper region of the annulus to the lower portion, resulting in a relatively thick down-flow region adjacent to the outer sphere. Following this action, the up-flow region adjacent to the inner sphere expands to a relatively large thickness to throw the fluid into the upper portion, thereby maintaining continuity.

There is no definite period of occurrence for the above described sequence of motion, and again the frequency of occurrence increases with Grashof number. This unsteady flow pattern is very similar to the falling vortices pattern previously observed by Bishop, Mack and Scanlan [2] and is therefore considered to be the same basic type of flow pattern. Thus, additional photographs of this pattern are not presented here.

All of the currently available information concerning natural convective flow patterns with air contained between isothermal concentric spheres is summarized in Fig. 7. The data points in this figure represent merely the extremes of the range of Grashof numbers which have been obtained for the particular inverse relative gap widths, D_i/L, studied. Inverse relative gap widths are used here rather than diameter ratios in order to expand and contract portions of the plot for greater ease in using the figure. Shaded bands are used to represent the transition from one type of flow pattern to another, and the Grashof number at the bottom of the band at any given inverse relative gap width indicates the point where a change in pattern type was first observed. These lines are given a finite thickness to indicate that the change from one type of pattern to another was not sudden but rather was gradual with increasing Grashof number.

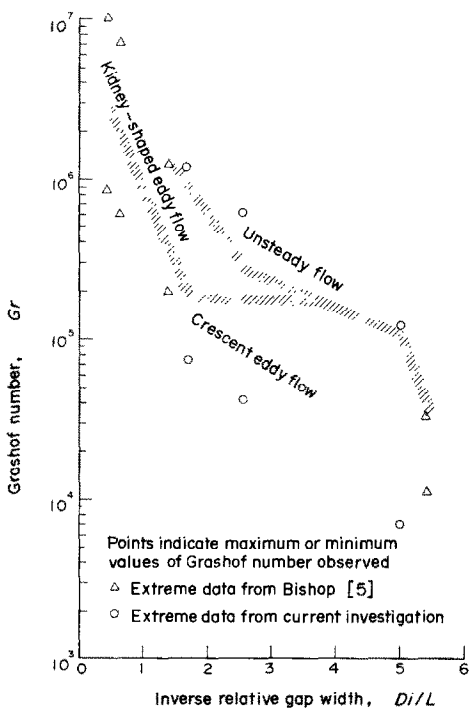

FIG. 7. Categorization of flow regimes for air.

From this figure it may be observed that, for inverse relative gap widths between about 0·45 and 5·4, the basic crescent eddy pattern occurs for small Grashof numbers. For inverse relative gap widths greater than about 3·7, this crescent eddy flow pattern changes directly to an unsteady flow pattern if the Grashof number is increased at a constant value of D_i/L. For the inverse relative gap widths which have been utilized in this region, 5·0 and 5·4, the unsteady flow pattern is a type of falling vortices pattern.

For inverse relative gap widths less than about 3·7, increasing the Grashof number at a constant value of D_i/L results first in a transition from the crescent eddy pattern to the kidney-shaped eddy pattern and finally in a transition to an unsteady pattern. For $0{\cdot}45 < D_i/L < 1{\cdot}7$ the Grashof number at which transition from the crescent eddy to the kidney-shaped eddy flow pattern occurs decreases sharply with increasing D_i/L, and this value of the Grashof number is relatively constant for $1{\cdot}7 < D_i/L < 3{\cdot}7$. For all inverse relative gap widths studied, the value of the Grashof number for transition from steady to unsteady flow decreases rather rapidly with increasing D_i/L.

The unsteady flow patterns observed for inverse relative gap widths of 1·7 and 2·53 are both characterized by changes in the central low-speed flow regions rather than in the outer high speed regions—the change occurring in the upper portion of the low-speed region for $D_i/L = 1{\cdot}7$ and in the lower portion for $D_i/L = 2{\cdot}53$. For $D_i/L < 1{\cdot}4$ Grashof numbers large enough to produce unsteady flows have not been attained.

For water as the gap working fluid, the basic flow pattern obtained for all sphere combinations at low Grashof numbers is illustrated in Fig. 8 for a diameter ratio of 2·17. This pattern may be described in terms of three distinct regions. First, a thin high-speed primary flow region is observed in the vicinity of each sphere. The fluid in this area moves upward along the inner sphere and downward along the outer sphere with a relatively high speed compared to that in

other portions of the gap. As with air, this motion results in a dividing line, or chimney, along the upward vertical axis.

Secondly, an interior, low-speed flow region is observed in the upper portion of the annulus. Here there are two secondary flows circulating in the same direction as the primary flow. One of them is attached to the inner sphere producing a weak return flow to the near vicinity of the inner sphere. The other appears at the extreme top of the gap adjacent to the chimney, and, evidently, a weak shear layer must occur between these two cells. Finally, the major part of the annulus consists of a central stagnant region in which the flow can be detected only by photographs using a relatively long time exposure.

The steady flow pattern described in the foregoing paragraphs was the only steady flow pattern observed for water as the test fluid. As in the case of air, an unsteady flow pattern occurs when the Grashof number exceeds a transition value for all sphere combinations utilized, and the exact nature of the unsteady flow was found to be dependent on the diameter ratio. It should again be noted that, for Grashof numbers only slightly above the transition value, very small deviations from steady flow were observed, but the unsteadiness became progressively more pronounced as the Grashof number was increased.

Consider first the largest diameter ratio utilized in the current investigation, 2·17. When the Grashof number is increased above a value of 3 600 000 for this sphere combination, the upper secondary cell is no longer stationary in position. Instead, this cell is alternately formed and then submerged into the relatively stagnant region of the upper interior portion of the annulus, thereby causing a somewhat random motion to occur. Simultaneously, fluid is also discharged from this region along the inner surface of the outer sphere with a rolling vortex motion. This flow phenomenon is repeated with an indefinite period, although the frequency appears to increase with Grashof number. The majority of the fluid in the annulus remains relatively stagnant, however. This flow pattern is illustrated in Fig. 9.

For a diameter ratio of 1·78, the steady flow pattern exists undisturbed until a Grashof number of 1 184 000 is reached. At this point, the weak shear region between the secondary cells expands and becomes a weak tertiary cell, and the upper secondary cell grows in size and changes in shape. On the other hand, the lower secondary cell is reduced in size, and most of the flow in this region returns to the outer sphere high speed layer instead of to the inner sphere layer, as was the case with the steady flow pattern. In addition, a considerable amount of random motion is observed in the interior low speed secondary flow region. This type of unsteady flow pattern is illustrated in Fig. 10.

For the two smallest diameter ratios considered, a type of falling vortices flow pattern, similar to that obtained in air, occurs for large Grashof numbers. This flow pattern is illustrated in Fig. 11 for a diameter ratio of 1·40. When the transition Grashof number is exceeded, the flow in the upper portion of the gap randomly alternates between a two-dimensional vortex motion and a three-dimensional spiral motion. Fluid is continually supplied to this region by flow separated from the upward primary flow along the inner sphere. It was observed that a continuous withdrawal of fluid from this upper region occurs through the portion nearest the outer sphere, and this withdrawn fluid combines with the primary flow to return to the lower portion of the annulus. Only a very slight sideways oscillation occurs in the upper regions, and, occasionally, the continuous withdrawal of fluid from the upper portion of the gap is enhanced by a slug of fluid generated in this vicinity. There is no definite period of occurrence for this phenomenon, however.

All of the currently available information concerning natural convective flow patterns with water contained between isothermal concentric spheres is summarized in Fig. 12. The data points in this figure, as in Fig. 7, represent merely the extremes of the range of Grashof

numbers which were obtained for the particular inverse relative gap widths studied. Shaded bands are used to represent the transition from a steady to an unsteady flow pattern, and the Grashof number at the bottom of the band at any inverse relative gap width indicates the point where an unsteadiness in the flow pattern was first observed. As in the case of air, these lines are given a finite thickness in order to indicate that the change from completely steady to completely unsteady flow was not sudden but rather was gradual with increasing Grashof number.

In Fig. 12, it may be observed that a single steady flow pattern occurs for all diameter ratios. This pattern was characterized in terms of three distinct regions: a high speed flow region, a secondary flow region, and a relatively stagnant region. The high speed flow region consists of relatively thin fluid layers immediately adjacent to both the inner and outer sphere surfaces. The secondary flow region is composed of two relatively small cells adjacent to the chimney in the upper portion of the gap with both cells rotating in the same direction as the high speed primary flow. The central, major portion of the gap is almost completely stagnant.

As the Grashof number is increased at a constant value of D_i/L, Fig. 12 indicates that an unsteady flow pattern will occur, and the characteristics of this unsteady pattern were found to vary with D_i/L. For an inverse relative gap width of 1·7, the unsteady flow consists basically of an alternate formation and disruption of the upper secondary cell. The unsteady flow pattern for an inverse relative gap width of 2·6 is characterized mainly by the formation of a tertiary cell in what had previously been the secondary flow region. Finally, for inverse relative gap widths of both 5·0 and 25·0, the unsteady flow is of a falling vortices type, similar to that observed in air. It should be noted that this is the only flow pattern observed in water which bore any resemblance to a flow pattern obtained in air. Since the ranges of values for the Grashof number and the inverse relative gap width were identical for both air and water, the differences in the observed flow patterns are due to the difference in Prandtl number ranges between the two fluids. In Fig. 12, as in Fig. 7, it may be observed that the transition Grashof number does decrease rather markedly with increasing inverse relative gap width.

Finally, it should be noted that the results of the current flow visualization study are in very good qualitative agreement with the results of a previous heat transfer investigation [4] using the same sphere combinations with both air and water as the gap fluids. Except for the largest inverse relative gap width utilized, 25·0, the ordering of the temperature profiles suggested the existence of steady unicellular flow patterns for small Grashof numbers. This was confirmed in the current investigation where the crescent eddy or the kidney-shaped eddy flow patterns were observed for small Grashof numbers with air, and, even though the steady flow pattern for water contained two small secondary cells, these would not have been detected by the upper thermocouple probes, which were located at 0° and 40° from the vertical.

Temperature fluctuations at larger Grashof numbers for all inverse relative gap widths [4] suggested the existence of unsteady flow patterns, and such patterns were indeed observed in the current investigation. The unusual ordering of the temperature profiles observed earlier for an inverse relative gap width of 25 led to the hypothesis of a multicellular flow pattern for this configuration. This earlier hypothesis is now verified by the discovery of the falling vortices pattern throughout the observable range of Grashof numbers for this geometry with water as the test fluid. Even though the falling vortices pattern occurred for Grashof numbers above the transition value, it could probably best be described as a quasi-steady pattern for Grashof numbers only slightly greater than that where transition occurred. Thus, it is reasonable to suppose that fluctuations would not have been detected in the temperature profiles for this

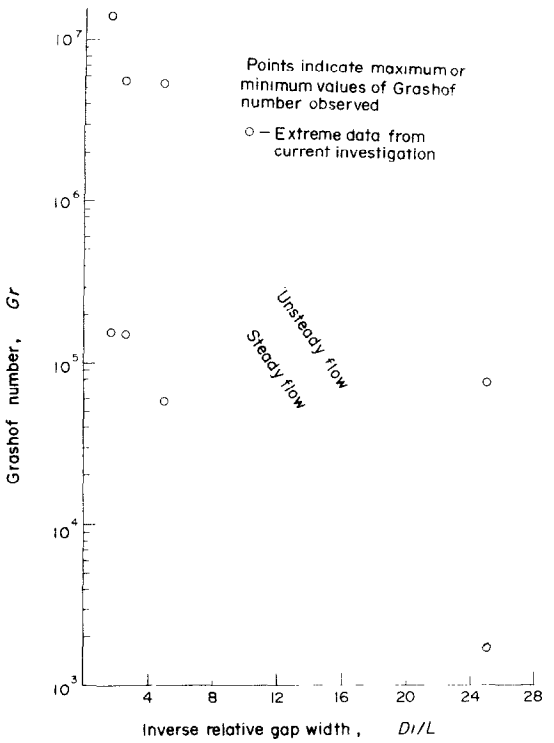

FIG. 12. Categorization of flow regimes for water.

pattern.

Finally, by comparing the current flow visualization results to the previous heat transfer results [4], it may be observed that the rate of increase of heat transfer with Grashof number is not affected significantly by transition from one type of flow pattern to another. If this were to occur, then distinct changes in slope of the heat transfer correlations at points where pattern changes occurred would be expected, but no such changes in slope were observed.

4. CONCLUSION

This paper reports the results of an experimental study of the natural convection flow patterns which develop in a fluid filling the annular space between isothermal concentric spheres. The fluids used were air and water, and in all cases the heat flux was from the inner to the outer sphere. Several different sizes of inner spheres were used with each fluid in order to determine the effect of annulus thickness on the types of flow pattern, and the temperature difference between the spheres was also varied in each case to determine the effect of driving potential on flow velocity and pattern.

All observations were made under steady-state boundary conditions; some of the resulting flow patterns were steady, and some were unsteady but of an essentially repetitious nature. It was found possible to categorize, and hence predict, the type of flow in terms of Grashof number and inverse relative gap width independently for each fluid.

Representative examples of still photographs are shown; the study also utilized motion picture photography and direct visual observation. The technique previously described [1] for making air flow patterns visible was used, and a new technique for use with water was developed and is described herein.

ACKNOWLEDGEMENTS

The work reported in this paper was supported by the Atomic Energy Commission under contract number AT (45-1)-2214 and by the National Science Foundation under grant number GK-31908.

REFERENCES

1. E. H BISHOP, R. S. KOLFLAT, L. R. MACK and J. A. SCANLAN, Convective heat transfer between concentric spheres, Proc. 1964 Heat Transfer Fluid Mech. Inst., pp. 69–80. Stanford Univ. Press.
2. E. H. BISHOP, L. R. MACK and J. A. SCANLAN, Heat transfer by natural convection between concentric spheres, *Int. J. Heat Mass Transfer* **9**, 649–662 (1966).
3. R. E. POWE, C. T. CARLEY and E. H. BISHOP, Free convective flow patterns in cylindrical annuli, *J. Heat Transfer* **91C**, 310–314 (1969).
4. J. A. SCANLAN, E. H. BISHOP and R. E. POWE, Natural convection heat transfer between concentric spheres, *Int. J. Heat Mass Transfer* **13**, 1857–1872 (1970).
5. E. H. BISHOP, Heat transfer by natural convection between isothermal concentric spheres, Ph.D. Dissertation, University of Texas, Austin (1964).
6. N. WEBER, R. E. POWE, E. H. BISHOP and J. A. SCANLAN, Heat transfer by natural convection between vertically eccentric spheres, *J. Heat Transfer* Series C, in press (ASME paper no. 72-WA/HT-2).

7. D J. BAKER, A technique for the precise measurement of small fluid velocities, *J. Fluid Mech.* **26** 573–576 (1966).
8. S. H. YIN, Natural convective flow between isothermal concentric spheres, Ph.D. Dissertation, Montana State University, Bozeman (1972).

FIGURES D'ECOULEMENT PAR CONVECTION NATURELLE DANS DES ANNEAUX SPHERIQUES

Résumé—On décrit une recherche expérimentale concernant des figures d'écoulement par convection naturelle qui se produisent dans l'espace annulaire entre deux sphères concentriques isothermes dont la plus petite est la plus chaude. Les rapports de diamètre varient entre 1,09 et 2,17. Les fluides convectifs sont l'air et l'eau. Les nombres de Grashof varient entre $1{,}7 \cdot 10^3$ et $1{,}5 \cdot 10^7$. Les divers types de figures d'écoulement observées sont reliés à des profils de température déjà publiés et sont classés en régimes stables ou instables.

STRÖMUNGSBILDER VON NATÜRLICHER KONVEKTION IN SPHÄRISCHEN RINGSPALTEN

Zusammenfassung—Eine experimentelle Untersuchung über Strömungsbilder der natürlichen Konvektion im Ringraum zweier konzentrischer Kugeln, deren innere eine höhere Temperatur aufweist, wird beschrieben. Die Durchmesserverhältnisse erstreckten sich von 1,09 bis 2,17. Konvektionsfluide waren Luft und Wasser in einem Bereich der Grashof-Zahlen von $1{,}7 \cdot 10^3$ bis $1{,}5 \cdot 10^7$. Die verschiedenen beobachteten Strömungsbilder wurden bereits früher veröffentlichten Temperatur-Profilen zugeordnet und nach stationären und nichtstationären Bereichen unterschieden.

РЕЖИМЫ ТЕЧЕНИЙ ПРИ ЕСТЕСТВЕННОЙ КОНВЕКЦИИ В СФЕРИЧЕСКОМ КОЛЬЦЕВОМ КАНАЛЕ

Аннотация—Экспериментально исследовалась картина течения при естественной конвекции в кольцевом зазоре между двумя изотермическими сферами, причем внутренняя сфера была нагрета сильнее. Отношение диаметров изменялось от 1,09 до 2,17. Рабочими жидкостями были воздух и вода. Число Грасгофа для них колебалось в пределе от $1{,}7 \times 10^3$ до $1{,}5 \times 10^7$. Показана связь наблюдаемых конфигураций течения с ранее опубликованными температурными профилями, и рассмотренные конфигурации течения классифицированы как стационарные или нестационарные.